THE ASTROPHYSICAL JOURNAL, 478:112–123, 1997 March 20

THE STELLAR CONTENT OF GIANT H II REGIONS IN NGC 7714

MARÍA LUISA GARCÍA-VARGAS,[1] ROSA M. GONZÁLEZ-DELGADO,[2] ENRIQUE PÉREZ,[2,3] DANIELLE ALLOIN,[4] ANGELES DÍAZ,[5] AND ELENA TERLEVICH[6]

Received 1996 June 11; accepted 1996 October 10

ABSTRACT

In this work we investigate the stellar content of three circumnuclear giant H II regions in the starburst galaxy NGC 7714. We model the stellar population that best reproduces the observational constraints given by the Hα image and the optical spectroscopy from 3710 to 9700 Å.

In this paper we address a robust method for analyzing the stellar content of giant extragalactic H II regions (GEHRs) as a first step in a strategy that should allow us to understand better how star formation proceeds. To test the power of the method, we have chosen three very well-studied regions in which many observational constraints are known. The models reproduce simultaneously the observed sizes derived from the Hα image, the emission-line spectrum from the gaseous component, and the optical features from the massive stars such as Wolf-Rayet bumps in emission, and the near-infrared calcium triplet, CaT, in absorption when detected.

We fit the stellar populations through evolutionary synthesis models plus the photoionization code CLOUDY, under the assumption of a *shell* geometry for the regions. This approach allows us to derive the physical properties of the star clusters, such as mass, age, and metallicity, inside these GEHRs. The method is based on previous work of a complete grid of photoionization models for giant H II regions ionized by evolving star clusters of different metallicities (from 0.05 to 2.5 times solar) and ages between 1 and 5.4 Myr. For the present work, we have followed the cluster evolution further, even after the ionization phase has come to an end, in order to reproduce the observed values of the continuum luminosity at 9000 Å and the equivalent widths of Hβ in emission and CaT in absorption.

From the results, we find in two of the three studied regions that a single ionizing stellar burst is sufficient to explain all the observational constraints if no reddening is affecting the cluster continuum. Otherwise, the observed values of the Hβ equivalent widths imply the existence of an older component. In this latter case, we find that a model in which two bursts of star formation are considered, a young ionizing one, with ages 3–5 Myr and an older one of 7–9 Myr, that can reproduce the observations. In the third region, the presence of CaT in the near-IR indicates the presence of a non-ionizing population, whose origin is thoroughly discussed.

Subject headings: galaxies: evolution — galaxies: individual (NGC 7714) — galaxies: ISM — galaxies: starburst — galaxies: stellar content — H II regions

1. INTRODUCTION

Much of the work published to date on the modeling of the emission-line spectra of giant extragalactic H II regions (GEHRs) based on photoionization codes (see, e.g., McCall, Rybski, & Shields 1985; Stasińska 1990) uses the atmosphere of a single star to represent the shape of the ionizing continuum. The H II regions modeled in this way can be characterized by three parameters—metallicity, effective temperature, and ionization parameter (Díaz et al. 1991; Díaz 1994). However, the high Hα luminosity in most GEHRs indicates the presence of a star cluster as the source of ionization, instead of a single star that suits most Galactic H II regions.

Previous attempts to construct more realistic models for GEHRs include the work by McGaugh (1991) who assumed zero-age clusters at different metallicity as the source of ionization. This type of model can reproduce H II regions photoionized by very young (essentially unevolved) star clusters whose integrated ionizing spectra are controlled by O–B main-sequence stars. However, when the most massive stars evolve, reaching high effective temperatures and luminosities, the situation changes very rapidly. Even a few evolved massive stars (in advanced Wolf-Rayet stages) can control the shape of the ionizing spectrum of the cluster, rendering the relationship between ionizing power and effective temperature meaningless (García-Vargas, Bressan, & Díaz 1994).

To improve the understanding of the impact of the stellar evolution on the emission-line spectrum of the surrounding nebula, García-Vargas & Díaz (1994) computed a set of models for GEHRs in which the effect of the cluster age was taken into account; these models were computed only for star clusters of solar metallicity. In a subsequent work, García-Vargas, Bressan, & Díaz (1995a, hereafter GBD95a) included the effects of metallicity and built a complete grid of photoionization models for GEHRs with abundances in the range from 0.05 to 2.5 times solar (see the results in García-Vargas, Bressan, & Díaz 1995b, hereafter GBD95b).

[1] INSA; ESA IUE Observatory, Villafranca del Castillo Satellite Tracking Station, P.O. Box 50727, 28080-Madrid, Spain; mgv@vilspa.esa.es.

[2] Space Telescope Science Institute, 3700 San Martin Drive, Baltimore, MD 21218; gonzalez@stsci.edu.

[3] Instituto de Astrofísica de Andalucía (CSIC), Aptdo. 3004, 18080 Granada, Spain; eperez@stsci.edu.

[4] Service d'Astrophysique, CEA Saclay, F-91191 Gif-sur-Yvette, France; alloin@ariane.saclay.cea.fr.

[5] Dpto. de Física Teórica. Fac. de Ciencias, C-XI. Cantoblanco. Univ. Autónoma de Madrid. 28049-Madrid, Spain; angeles@astro1.ft.uam.es.

[6] Institute of Astronomy, Madingley Road, Cambridge CB30HA, UK; et@ast.cam.ac.uk.

Recently, Stasińska & Leitherer (1996) have used the same approach to compute a grid of models for H II galaxies.

GBD95a devised an observational method to constrain the physical properties—mass, age, and metallicity—of the star clusters that ionize GEHRs, using diagnostics based on the optical emission-line spectrum of the ionized gas. The models also provide information about the relative number of massive stars in the cluster. In the present paper, we apply this method to analyze three GEHRs in the circumnuclear zone of the starburst galaxy NGC 7714.

NGC 7714 was classified as a typical starburst galaxy (Weedman et al. 1981) with a very bright nucleus. The Hα and *IRAS* luminosities indicate that the galaxy is experiencing a burst of star formation, being more conspicuous in the central part of the galaxy, where the star formation rate per unit area is twice that obtained for the galaxy as a whole (González-Delgado et al. 1995, hereafter G95). Evolutionary synthesis models by Bernlöhr (1993) point to a star formation process having occurred continuously in the nucleus for the last 20 Myr.

This galaxy has been considered as a good candidate to study in detail any possible connection between nuclear activity and star formation, and very detailed studies have been carried out in the optical and near-IR part of the spectrum in the frame of the ongoing work of the GEFE collaboration.[7] This study was focused on the characterization of both the gas properties in the nuclear and circumnuclear regions (see G95 and references therein) and the physical properties of the young clusters able to produce the emission-line spectrum of the gas, which is the goal of the present work. The data and main properties of the GEHRs studied in this work can be found in G95. Following this earlier work, we will refer to these regions as A, B, and C (see Fig. 1*c* of G95). Regions B and C are located in the disk of the galaxy 12″ northwest and 14″ southwest of the nucleus respectively. Region A is located at only 5″ southeast of the nucleus (945 pc for a distance of 39 Mpc; Demoulin 1968) in the rising, solid body part of the velocity curve (see Figs. 6*a* and 15*a* of G95).

The three regions have Hα luminosities of the order of 10^{40} ergs s^{-1}, which imply masses of the ionizing clusters of the order of 10^5 $M_\odot$ if a standard initial mass function (IMF) is assumed (see G95). Regions B and C have a metallicity 0.20 times solar, while region A has a somewhat higher metallicity, 0.35 times solar, similar to that of the nucleus of the galaxy.

We stress the need for high-quality data to carry out this kind of study. The full optical emission-line spectrum is required to derive the physical parameters of the ionized gas (density, temperature, and ionization parameter) and the chemical composition. Also, Hα imaging is required to compute the number of ionizing photons and to define the *core* radius of the emitting region, as discussed later in § 4.

Section 2 of this paper summarizes the main properties of the evolutionary synthesis and photoionization models that are discussed in detail in GBD95a and GBD95b. Section 3 is devoted to the derivation of the ionizing stellar population in the studied regions. Section 4 describes the photometric technique used to measure the sizes of GEHRs and presents a physical interpretation of the core radius, relating it to that of a bubble driven by the mechanical energy from the winds of the young embedded star cluster. Section 5 discusses if the models reproduce the rest of observational constraints. In particular, the number of Wolf-Rayet stars is discussed in § 5.1. The Wolf-Rayet content is analyzed from the emission features at $\lambda\lambda$4660, 5810, which are then compared to the model predictions. Section 5.2 discusses the observed values of the equivalent width of Hβ in emission, EW(Hβ), the continuum luminosity at 9000 Å (L_{9000}), and the equivalent width of the CaT absorption lines, EW(CaT). To reconcile these observations with models, two possibilities are argued: a single ionizing burst without dust associated with the stellar component or the coexistence of two populations, and a young ionizing burst plus an older non-ionizing one with an age about 7–12 Myr. Finally, § 6 summarizes the results.

2. SUMMARY OF THE MODELS

The models used in this work are those of GBD95a. In this section, the main characteristics of the evolutionary synthesis and photoionization models are outlined. A full description can be found in the original paper of GBD95a. Since the choice of the stellar tracks and atmosphere models for massive stars are crucial hypotheses in the models, we refer the reader to the review by García-Vargas (1996 and references therein) in which the influence of the stellar evolution and atmosphere models on photoionization is analyzed and discussed in detail.

In the models it is assumed that a single burst, formed with a standard IMF (Salpeter 1955) between the stellar mass limits 0.85 $M_\odot$ and 120 $M_\odot$, is the dominant stellar population in these GEHRs.

The basic properties of the H-R diagram for a given ionizing cluster are obtained by constructing isochrones at several ages interpolating between the stellar evolutionary sequences calculated by the Padova group (Bressan et al. 1993; Fagotto et al. 1994a, 1994b, and references therein). In the models, the pre–main-sequence evolution is not taken into account. The tracks include mild overshooting from the convective core, as introduced by the formalism of Bressan, Bertelli, & Chiosi (1981), and the radiative opacities by Iglesias, Rogers, & Wilson (1992) are used.

The mass-loss rate via stellar winds is the parameter that dominates the evolution of massive stars, and it has been accounted for according to the rates given by de Jager, Nieuwenhuijzen, & van der Hucht (1988) from the main sequence up to the so-called de Jager limit in the H-R diagram. They include the dependence on metallicity given by Kudritzki, Pauldrach, & Puls (1987). Beyond the de Jager limit, the most massive stars enter the region where luminous blue variables (LBVs) are observed, and, accordingly, the mass-loss rate has been increased to 10^{-3} $M_\odot$ yr^{-1} in the Padova models. As the evolution proceeds, the surface hydrogen abundance by mass in the most massive stars eventually falls below the value of 0.3. In this case the model is supposed to produce a W-R star. For the W-R phase, the mass-loss rate is derived according to Langer (1989).

The study of GBD95a, based on the Padova models, shows that at low metallicities, the mass-loss rate is less efficient and, as a consequence, the number of W-R stars at a given age is a decreasing function of the metallicity. The distribution of W-R stars among the different subtypes

[7] GEFE (Grupo de Estudios de Formación Estelar) is an international collaboration of astronomers formed to take advantage of the international time granted by the Comité Científico Internacional at the Observatories in the Canary Islands.

reflects the interplay between the mass-loss rate, which is metal dependent, and the behavior of the convective core, which determines the inner chemical profile (see also Maeder 1991). In the Padova models, the W-R phase has a maximum in duration and in number ratios of W-R to stars more massive than 20 $M_\odot$ at solar metallicity, although the phase is seen in bursts with metallicities between 0.2 and 2.5 $Z_\odot$.

Two different sets of stellar atmosphere models were used to compute the SED: those of NLTE models by Clegg & Middlemass (1987) for stars with $T_{\rm eff} \geq 50{,}000$ K (corresponding to the last evolutionary stages of massive stars, W-R) and those by Kurucz (1992) for stars with 3500 K $\leq T_{\rm eff} < 50{,}000$ K. Reasons for the choice of these specific models are given in García-Vargas & Díaz (1994) and GBD95a. A comparison between the synthesized spectra used here and those from Leitherer & Heckman (1995), who also used NLTE models for W-R stars but took into account stellar winds, shows that both are suitable to describe the SED of a young starburst (García-Vargas 1996).

In the present work, the metallicity of the stars has been taken to be similar to that of the gas, and therefore we have used those SEDs from GBD95a (see Fig. 3 in GBD95a) corresponding to metallicities $Z = 0.004$ (0.2 times solar) in regions B and C and $Z = 0.008$ (0.4 solar) in region A.

If the cluster is young enough to ionize the surrounding gas and form an H II region, the synthesized SED is used as input for the photoionization code CLOUDY (Ferland 1991) to obtain the corresponding emission-line spectrum. The H II region is assumed to be ionization bounded.

The ionized gas is assumed to be located in a thin spherical shell at a distance R_u from the ionizing source. The ratio of the shell thickness to its radius is small enough that the model is effectively described by a *plane-parallel* geometry.

The radius of the ionized zone can be fixed through the definition of the ionization parameter u, given by the equation

$$u = Q(\mathrm{H})/4\pi c R_u^2 n_{\rm H}\,, \qquad (1)$$

where Q(H), the number of ionizing photons, can be derived from the Hα luminosity; $n_{\rm H}$, the hydrogen density, is taken equal to the electron density, derived from the [S II] 6717/6731 Å quotient; and u, the ionization parameter, can be estimated from suitable emission-line ratios. In our case, the [S II]/Hα or [S II]/[S III] ratios, depending on metallicity, have been used.

A numerical calibration between the ionization parameter, u, and the ratio of the sulfur lines as a function of the gas metallicity was discussed in GBD95a. The fits for this calibration included a series of models computed with ages between 1.5 and 5.4 Myr, and a wide range in u.

The following equations (see GBD95a for more details) summarize the calibrations for the metallicities used in this paper, equation (2) for region A and equation (3) for regions B and C:

$$\log u = (-1.18 \pm 0.02) r_1 + (-3.08 \pm 0.01); \quad Z \geq 0.008 \qquad (2)$$

$$\log u = -0.80 r_2^2 - 3.30 r_2 - 4.86; \quad Z = 0.004 \qquad (3)$$

where $r_1 = \log$ ([S II] 6716 + 6731/[S III] 9069 + 9532), and $r_2 = \log$ ([S II] 6716 + 6731/Hα).

3. FROM GAS TO STARS: UNVEILING THE IONIZING CLUSTER

The goal of this paper is to study the stellar population inside GEHRs. The process we have followed is illustrated in Figure 1. Once the main properties of the gas—electron density, electron temperature, and metallicity—and the stellar cluster—number of ionizing photons—have been derived, the spectral energy distribution (SED) of the clusters whose ages are roughly consistent with the optical nebular spectrum and the presence or absence of W-R features are used as input for the photoionization code. Several iterations are performed, slightly modifying the cluster age and the ionization parameter, until a consistent agreement is found between the predicted and observed intensities for the brightest optical emission lines. The error in the relative ages determined in this way is of the order of 0.5 Myr, although the absolute value depends on the chosen stellar evolutionary models.

The electron density and nebular abundances of the three studied regions have been taken from G95 and are summarized in Table 1. Electron densities are of the order of 100 cm^{-3}. Abundances are derived for O, S, N, Ne, and He, except in the case of region A where the He abundance could not be calculated. An abundance of He/H of 0.081 by number, similar to the one derived for the other two regions, was required in order to reproduce the observed value for the He I 4471 Å line.

The number of ionizing photons, Q(H), has been computed from the reddening corrected Hα luminosity (Osterbrock 1989) derived from the Hα image (the reddening constant derived from the spectroscopy for region A was used). The errors in Q(H) have been derived assuming photon noise plus an estimate of the uncertainty introduced by the subtraction of the continuum image from the Hα + continuum image. The major contribution to this error comes from the uncertainty on the area occupied by the H II region and the background noise. These errors are only lower limits since the uncertainties introduced by the flux calibration (only one spectrophotometric standard was observed), and the continuum subtraction are difficult to evaluate.

Finally, the ionization parameter has been estimated from the [S II]/Hα ratio for regions B and C and from [S II]/[S III] ratio for region A. It might be questioned whether photoionization models correctly predict the sulfur line

TABLE 1

OBSERVED PROPERTIES OF THE GEHR IN NGC 7714

Region	log n_e	O/H	S/H	N/H	Ne/H	He/H
A.....	2.22 ± 0.08	8.5 ± 0.2	6.7 ± 0.1	7.6 ± 0.3	7.8 ± 0.3	...
B.....	2.04 ± 0.04	8.2 ± 0.2	6.4 ± 0.1	7.2 ± 0.2	7.5 ± 0.2	0.083 ± 0.002
C.....	1.98 ± 0.07	8.3 ± 0.3	6.5 ± 0.2	7.1 ± 0.4	7.6 ± 0.4	0.081 ± 0.009

NOTE.—All the abundances given as 12 + log(X/H), where X/H is given by number.

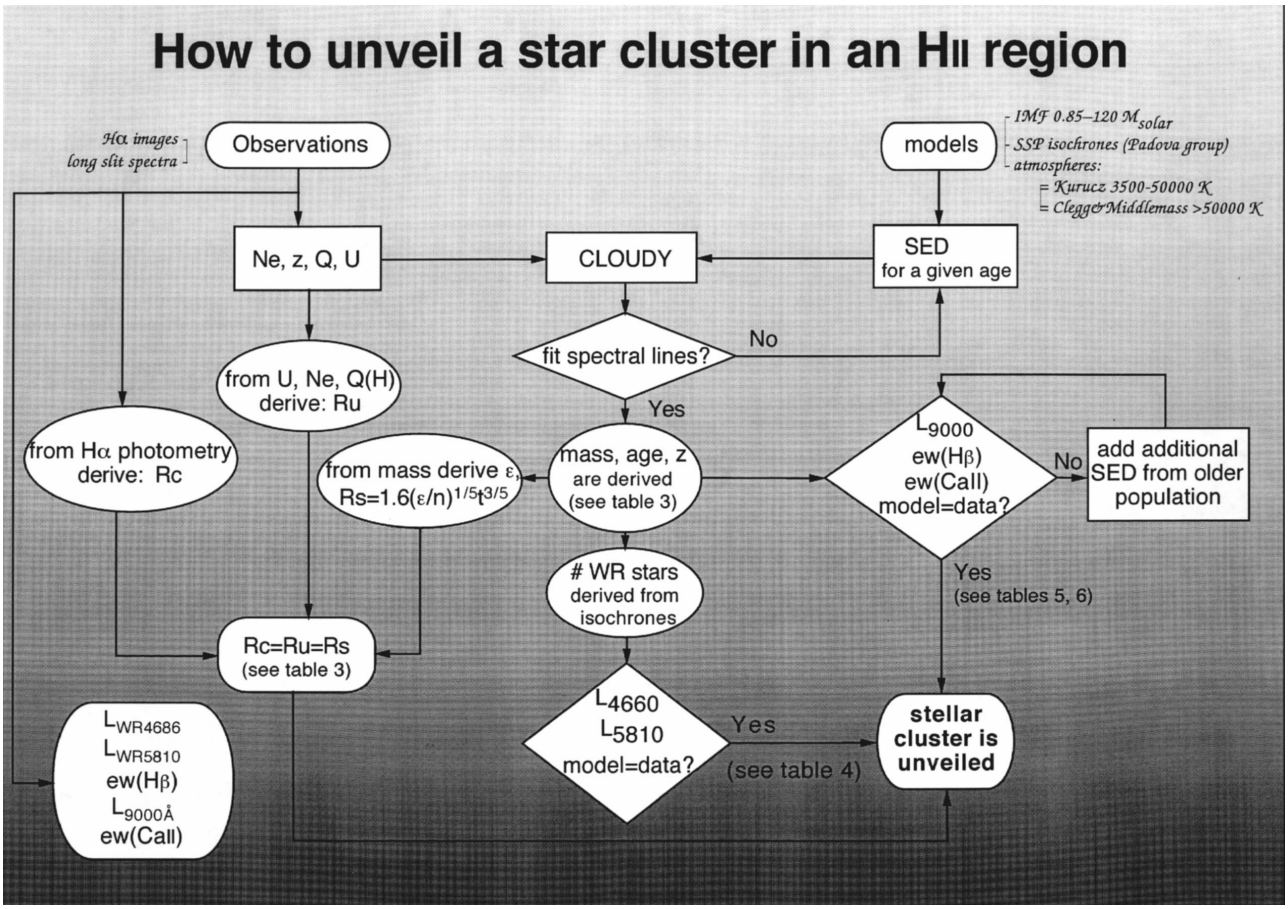

FIG. 1.—Flow chart of the process followed to study the stellar populations in GEHRs

intensities because of accuracy with which the atomic data are known (Garnett 1989). However, it should be noted that in our models, the ionization parameter is treated as a functional parameter and is used as a tool to obtain the age of the cluster by an iterative process. In fact, the finally adopted ionization parameter may actually differ from the one initially estimated on the basis of the sulfur line ratios.

We need only an estimation of log u to select a first model and, in an iterative process, to constrain the age of the ionizing cluster, which is the goal of this exercise. Moreover, log u could also be determined from other estimators, such as the line ratios [O II] 3727 + 3729/Hβ or [O II]/[O III] ratios. According to our models, the difference between ionization parameters derived from the various estimators is of the order of 0.2 dex at metallicities lower than 0.3 times solar. The trick is to use consistently the models with the calibration between the functional parameter, log u, and the age of the cluster. The only reason for which we have selected the sulfur lines is that the [S II]/Hα ratio is less reddening-dependent than the [O II]/Hβ and therefore the observational errors due to this effect will be smaller, and, consequently, a better determination of the first input for log u will ease the convergence of the iterative process.

In the case of regions with O/H abundance higher than 0.4 times solar (such is the case of region A), the [O III] lines are weaker, very metal-dependent, and also less sensitive to the ionization parameter, and the [S II]/[S III] ratio seems to be the best choice, from a theoretical point of view. However, the observed values of [S III] lines have larger associated errors owing to the difficulty in the data reduction of the near-IR part of the spectrum, e.g., the atmospheric absorption correction (Stevenson 1994). We have corrected from atmospheric absorption, dividing by the normalized spectrum of a standard star, which was observed just after the galaxy. In our case, the ratios [S III] 9069/[S III] 9532 are 2.84, 2.46, and 2.23 in regions A, B, and C respectively, differing only 9%, 6%, and 14% from the theoretical ratios, thus showing that the above problem is well constrained (see GD95 for the details of the data reduction).

The fixed inputs for the photoionization code are then (1) the hydrogen density, n_H taken to be equal to the electron density; (2) the O, S, N, Ne, and He abundances, which are allowed to vary within the limits given by the observational errors from the spectra (all other abundances are scaled to oxygen according to the solar ratio); (3) the number of ionizing photons, Q(H); and (4) the ionization parameter, log u, calculated from the emission-line ratios (eqs. [2] and [3], above).

From an inspection of the results given in GBD95a, we select an initial grid of SEDs for clusters whose ages are grossly consistent with the optical nebular spectrum (see below) and the presence or absence of W-R features. As the output, we obtain the intensity of the main emission lines, which are then compared iteratively to the observed values.

The age of the cluster is determined by running CLOUDY with different SEDs in order to fit simultaneously a total of 11 optical emission lines: [O II] 3727, [O III] 4363, 5007, He I 4471, 5876, [O I] 6300, [N II] 6584, [S II] 6717, 6731, and [S III] 9069, 9532.

TABLE 2

OPTICAL EMISSION-LINE SPECTRUM FITTING

Line λ (Å)	Region A	Model A	Region B	Model B	Region C	Model C
[O II] 3727	2.45 ± 0.02	2.45	2.42 ± 0.04	2.43	2.8 ± 0.3	2.95
[O III] 4363.....	0.017 ± 0.003	0.012	0.031 ± 0.005	0.043	0.017 ± 0.004	0.021
He I 4471	0.037 ± 0.002	0.039	0.030 ± 0.003	0.038	0.035 ± 0.004	0.037
[O III] 4959.....	0.453 ± 0.004	0.45	1.19 ± 0.01	1.19	0.86 ± 0.01	0.86
[O III] 5007.....	1.341 ± 0.008	1.34	3.57 ± 0.02	3.57	2.57 ± 0.03	2.57
He I 5876	0.105 ± 0.002	0.11	0.105 ± 0.003	0.107	0.11 ± 0.01	0.11
[O I] 6300	0.071 ± 0.002	0.03	0.064 ± 0.001	0.04	0.049 ± 0.005	0.03
[N II] 6548	0.306 ± 0.003	0.30	0.140 ± 0.003	0.13	0.12 ± 0.01	0.12
[N II] 6584	0.88 ± 0.02	0.89	0.378 ± 0.007	0.39	0.36 ± 0.04	0.37
[S II] 6717	0.419 ± 0.004	0.41	0.306 ± 0.006	0.30	0.33 ± 0.04	0.33
[S II] 6731	0.325 ± 0.003	0.32	0.224 ± 0.005	0.225	0.24 ± 0.03	0.25
[S III] 9069	0.208 ± 0.004	0.21	0.142 ± 0.005	0.26	0.13 ± 0.03	0.23
[S III] 9532	0.590 ± 0.01	0.55	0.35 ± 0.02	0.68	0.29 ± 0.07	0.60
[S III] 9069(*).....	8.00 ± 0.15	11.4	14.2 ± 2.7	14.1	13.0 ± 0.5	12.5
[S III] 9532(*).....	11.1 ± 0.2	15.1	17.5 ± 2.5	18.6	13.8 ± 1.0	16.4
log L(Hα)	40.2	40.2	40.1	40.1	40.2	40.2
log Q(H)	52.36	52.4	52.20	52.2	52.30	52.3
log u	−3.0 ± 0.2	−3.1	−2.9 ± 0.2	−2.9	−3.0 ± 0.2	−2.9

NOTE.—Observed values have been taken from G95 and correspond to the reddening-corrected line ratios. The reddening constant C(Hβ) was deduced from the Balmer line ratios, Hα/H$_\beta$, Hγ/Hβ. In the case of region A, a correction of 2 Å in the equivalent widths was included to take into account the underlying population contribution. The value of Q(H) corresponds to the one derived from the Hα image. All the line ratios are given relative to Hβ with the exception of the [S III] lines, marked with asterisks, at 9069 Å and 9532 Å, which are given relative to the near-IR Paschen lines Pa10 and Pa8, respectively, in order to avoid reddening effects when data and modeled values are compared (see text, § 3).

We have chosen only the strongest emission lines to represent the most relevant ionization stages and elements, and therefore we have selected the lines whose ratio to Hβ was larger than 0.3 with the exception of [O III] 4363 Å, which we have included owing to its importance for the electron temperature determination.

Table 2 shows the best fits obtained for the emission lines in the spectra of the three GEHRs. The corresponding cluster ages are given in Table 3.

The differences between the observations and the model predictions are less than 5%, except in the case of [O III] 4363 (difference of the order of −30% for region A and +30% for regions B and C), and [O I] 6300 (difference 50% for the three regions). The assumption of a unique density could account for part of the discrepancy since both lines have a large critical density and come mainly from the denser parts of the H II region (see, e.g., Pelat, Fosbury, & Alloin 1981). On the other hand, [O I] 6300 has been found to be enhanced in 30% of the H II galaxies studied by Stasińska & Leitherer (1996) with respect to the values predicted by photoionization models. According to these authors, this enhancement could be due to the presence of shocks as the result of the stellar evolution.

Regarding the sulfur lines, we consider more reliable the use of [S II] 6717, 6731, instead [S II] 4068, 4076 to represent the [S II] lines. Several reasons can be argued. On the one hand, [S II] 6717, 6731 are much stronger (a factor of 70) than the blue [S II] lines, which are actually very weak. On the other hand, these blue lines are located in a very reddening-dependent spectral range (although the baseline respect to Hβ is shorter). [S II] 4068, 4076 are very weak in the studied regions. Note that in GD95 the intensity of the two lines is given together in regions A and C, and it is impossible to measure in the case of region B.

The computed values for [S II] 4068 + 4076, normalized to the Hβ intensity, are 0.030 and 0.034 for regions A and C, respectively, while the observations give 0.024 and 0.034, which are in good agreement.

For the [S III] lines, the one at 6312 Å is even weaker, 0.008, 0.014, and 0.010 in regions A, B, and C, respectively (a factor of 60–70 weaker than the near-IR lines). The computed values are 0.010, 0.023, and 0.016 for regions A, B, and C, respectively. This result is quite good, considering the weakness of the lines.

The apparent discrepancies between computed and observed [S III]/Hβ ratios deserve special attention since they reach a factor of 2 in regions B and C. Similar discrepancies between the predicted and the observed [S III] fluxes have already been found in other high-metallicity giant extragalactic H II regions (G95; González-Delgado & Pérez 1996), as well as in active galactic nuclei (Osterbrock, Tran, & Veilleux 1992). It has been suggested that this discrepancy could be due to the above-mentioned uncertainties in the atomic parameters for sulfur. However, the long baseline between Hβ and the [S III] lines makes the [S III] 9069/Hβ and [S III] 9532/Hβ ratios to be very reddening and/or flux calibration dependent. A reasonable agreement is found between the measured and predicted ratios of

TABLE 3

PHYSICAL PARAMETERS OF THE IONIZING STAR CLUSTERS

Region	Z ($Z_\odot$ = 0.02)	Age (Myr)	Mass (10^4 $M_\odot$)	ϵ (10^{40} ergs s^{-1})	R_s (pc)	R_u (pc)	R_c (pc)
A.....	0.008	5.0 ± 0.5	224 ± 42	3.66	196 ± 32	201 ± 86	250 ± 50
B.....	0.004	3.5 ± 0.5	32 ± 3	0.39	112 ± 21	163 ± 62	250 ± 50
C.....	0.004	4.5 ± 0.5	91 ± 8	0.40	172 ± 27	218 ± 91	350 ± 70

[S III] 9069/Pa10(9014) and [S III] 9532/Pa8(9546) (see Table 2) which give differences of +42%, −1%, and −4% for the ratio [S III] 9069/Pa10 and +36%, +6%, and +19% for the ratio [S III] 9532/Pa8 in the regions A, B, and C, respectively. This suggests that both theoretical and observational uncertainties possibly contribute to the [S III] disagreement, and it may be safer to use the ratios of the [S III] to Paschen lines when comparing with values predicted by models.

Once the age is obtained, the mass of the ionizing cluster has been derived from the value of the number of photons per solar mass as a function of age and metallicity (GBD95b) assuming a Salpeter IMF ($\alpha = 2.35$) between 0.85 and 120 $M_\odot$. These masses are also given in Table 3. The mass that would be derived if the upper mass limit was lowered to 100 $M_\odot$ would be only 10% higher.

With the data we have used, i.e., the total number of ionizing photons via the observed Hα emission, it is not possible to constrain the lower limit of the IMF. In fact, only through studies of the stellar velocity dispersion could the total mass of the cluster, and hence the lower limit cut-off of the IMF, be determined.

However, we can evaluate the error introduced in the total mass determination owing to the uncertainty in this parameter. For $\alpha = 2.35$ and $m_{\rm up} = 120\ M_\odot$, the mass fraction in massive stars (more massive than 20 $M_\odot$) relative to the total cluster mass is 7% if $m_{\rm low} = 0.10\ M_\odot$ and 33% if $m_{\rm low} = 3\ M_\odot$ (the numbers are lower if we consider a lower value of $m_{\rm up}$ or a higher value of α). Therefore, if M_T is the total cluster mass derived from our assumed IMF parameters, it would be $0.6 \times M_T$ if $m_{\rm low} = 3\ M_\odot$ or $2.4 \times M_T$ if $m_{\rm low} = 0.1\ M_\odot$. However, all the parameters derived in this work, except the continuum luminosity at 9000 Å, are sensitive only to the massive stars, and the effect of changing $m_{\rm low}$ is minimum.

On the other hand, our models assumed that the nebula is ionization bounded and that the presence of dust is unimportant. If the nebula was matter bounded and/or if dust would be present, part of the ionizing photons would not be accounted for by using the Hα emission and the value of the mass derived from Q(H) would be underestimated. In summary, the uncertainties regarding the value of the IMF lower limit cutoff and the extinction by dust imply that the total mass estimates should be used only as a normalization factor.

4. ON THE SIZE OF GEHRs

4.1. *Observational Considerations*

Measuring the size of an H II region from an image is a somewhat arbitrary process, which involves fundamental and technical uncertainties. Although, in theory, we could characterize the size of an H II region by its Strömgren radius, in practice, observed ionization-bound GEHRs show a compact bright core plus an extended faint halo structure; this structure is produced by a combination of the density structure of the gas and the distribution of ionizing stars. For relatively isolated regions, the extent over which we observe the halo depends on the depth of the exposure. Some authors consider only the core when providing the size of the region, because the core often contains most of the flux; however, even this procedure involves some arbitrary choice, given that the transition between the core and the halo is not always a clear-cut case. On the other hand, if we were to use the external halo as indicative of the H II region size, we would be biasing the numbers toward large values: the halo contributes most of the region's size but at a much lower flux level than the core.

To avoid these uncertainties partly, we have developed a simple numerical algorithm that weights the contribution of each subsequent incremental radius to the final size of the region. It is the surface brightness of each incremental ring that is used as a weight. Thus, the inner parts of the region, which contribute most of the flux, are given a larger weight in the computation of the surface area of the region than the outer and fainter parts. A full account of the method is given in Pérez et al. (1997), and we briefly describe it here.

In practice we proceed as follows. We perform isophotal (as opposed to fixed geometry) aperture photometry on the Hα image of the H II region at a number of isophotal levels. The actual number of levels is chosen, for each region, so as to sample sufficiently well, in logarithmic flux increments, from the inner few core pixels to the detection limit. For each level, we compute the total Hα flux and the area enclosed. The equivalent radius is computed as $(\text{Area}/\pi)^{1/2}$. Thus, we have a curve of growth of the Hα flux versus the size. We then compute the following function:

$$\Phi = r \frac{dF}{dA}, \tag{4}$$

where F is the flux measured within the contour level of area $A = \pi r^2$, and dF and dA are the incremental flux and incremental area contributed by the next isophotal level. It can be shown (Pérez et al. 1997) that Φ always has a maximum for well-behaved $F(r)$, i.e., those with a general monotonic decrease. This maximum value is taken to be the *core* radius, R_c, of the GEHR. Figure 2 shows the curves of growth for the three regions in NGC 7714, labeled as A (*open circles*), B (*filled circles*), and C (*squares*). The values for R_c are listed in the eighth column of Table 3. The errors in R_c were estimated to be about 20%.

4.2. *Theoretical Considerations*

In their pioneering work, Castor, McCray, & Weaver (1975) demonstrated how an early-type star with a strong stellar wind can blow out a large cavity or "bubble" in the surrounding circumstellar medium, assuming that the swept-up circumstellar gas is compressed into a thin spherical shell.

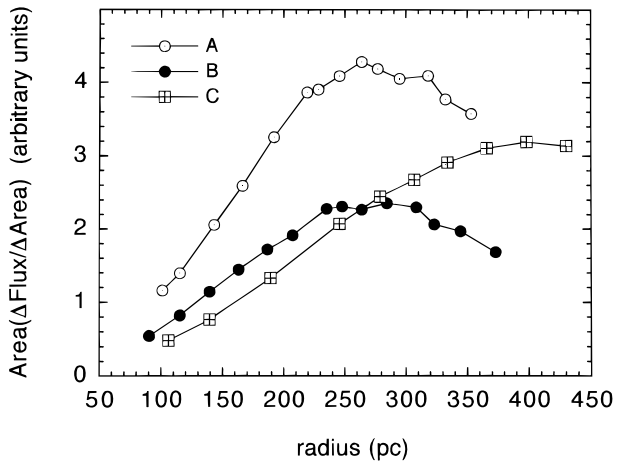

FIG. 2.—Surface brightness weighted radii for three GEHRs in NGC 7714, as measured from the Hα image. See text (§ 4) for details.

The evolution of such a wind-driven circumstellar shell can be sketched in the following way: It begins with an initial phase of free expansion and a phase of adiabatic expansion (Avedisova 1972; Falle 1975), followed by a phase in which the swept-up material collapses into a thin, cold shell as a result of radiative cooling (Cox 1972). At this stage the gas traps the ionization front and the radiative phase begins, during which ionizing photons are absorbed and the region cools via emission in the Balmer lines. During this process, the radius of the outer shock, R_s, evolves in time as $(\epsilon/n)^{1/5}t^{3/5}$ (Castor et al. 1975; Weaver et al. 1977), where ϵ is the mechanical energy per unit time injected by the wind, n is the interstellar medium density, and t the age of the shell.

The equation that describes R_s can be written as

$$R_s = 1.6(\epsilon/n)^{1/5}t^{3/5} \text{ pc}, \quad (5)$$

where ϵ is in units of 10^{36} ergs s^{-1}, n is in units of cm^{-3}, and t is iin units of 10^4 yr (Dyson 1979).

We suggest extrapolating this "bubble" geometry to a shell structure formed by the combined effects of the mechanical energy deposition from the winds coming from massive stars in the ionizing cluster. The resulting energy deposition rates from an evolving instantaneous burst have been calculated by Leitherer, Robert, & Drissen (1992) and Leitherer & Heckman (1995). We have used their models at $Z = 0.25\ Z_\odot$ and $Z = 0.5Z_\odot$ scaling ϵ to the total mass of the cluster responsible for the ionization of each selected GEHR (as derived from the number of ionizing photons through the reddening-corrected Hα luminosity). We have taken into account the normalization factor introduced by differences in the IMF parameters $m_{\rm low}$ and $m_{\rm up}$ in the two sets of models (1 $M_\odot$ and 100 $M_\odot$ in Leitherer & Heckman 1995, and 0.85 $M_\odot$ and 120 $M_\odot$ in GBD95a and GBD95b).

The fifth column in Table 3 lists the value of the mechanical luminosity. The sixth column lists the outer shock radius, R_s, calculated from equation (5), whose uncertainty has been derived according to a standard error propagation. The seventh column lists the inner shell radius, R_u as given by the definition of the ionization parameter (eq. [1]). Our ionization parameter values are derived from expressions involving the sulfur lines. However, as mentioned in § 3, the difference between these values and those derived from other line ratios is within 0.2 dex. Therefore, we have taken our derived value and assumed an error of ± 0.2 dex in log u. The error in the electron density has been taken from Table 1, and the uncertainty in the number of ionizing photons has been considered to be 20%, although this is only a lower limit. Taking into account these considerations, the error in R_u has been calculated by the error propagation in equation (1). Finally, the eighth column gives the core radius, R_c, derived from the photometrical analysis as discussed above. The three values, R_s, R_u, and R_c, are compatible within the errors.

There are some observations that point against this simple geometry. In fact, images of GEHRs in nearby galaxies exhibit a more complex structure. In particular, some of them show the presence of ionized filaments, loops, and shells that are often interpreted as resulting from the action of massive stars on their surroundings by winds and/or supernova explosions. This is the case of some GEHRs in M33 (Courtes et al. 1987; Hunter 1994), M31 (Hunter 1994), and the LMC (Rosado et al. 1996). Recently, Hunter, Boyd, & Hawley (1995) have reported observations of GEHRs that imply stellar productions exceeding the ionization requirements of the nebulae. They have suggested that a large fraction of the ionizing photons is escaping from the H II region into the surrounding interstellar medium of the galaxy. Leitherer et al. (1996) find that the number of ionizing Lyman-continuum photons deduced from the Hα luminosity in the central starburst of NGC 4214 is 4 times smaller than that computed from the number of hot massive stars, as deduced from the ultraviolet P Cygni profiles, and conclude that a significant fraction of ionizing photons escape from the H II region. However, this could be due to the small aperture, probably unable to contain all the Hα flux associated with the cluster.

We do not think that these concerns apply to the three GEHRs studied in this paper. The existence of strong [O I] lines and the low filling factors associated to the regions support the *shell geometry*. First, in all three regions, the [O I] 6300, 6363 lines are measured to be relatively strong (see Figs. 3, 4, and 5, and Tables 3A and 3B in G95), which is consistent with radiation-bound regions. Second, if the region were almost empty, the filling factors should be small. This is indeed the case for the three observed regions for which the ratio of the volumes given by the Strömgren sphere and the actual size of the region are 0.0008, 0.002, and 0.003 for regions A, B, and C, respectively. These values are similar to those found in other GEHRs. However, these two facts are insufficient because on the one hand, the intensity of the [O I] lines may be also enhanced owing to nonphotoionization processes, such as shocks associated with the stellar winds (Stasińska & Leitherer 1996) and, on the other hand, the low values of the filling factors are also compatible with the existence of dense filaments. Nevertheless, the strongest argument for defending the proposed *shell geometry* is discussed in next section, and it is the good agreement found between the numbers of massive stars derived following three different methods: (1) counting the ionizing photons necessary to reproduce the observed nebular spectrum, (2) fitting W-R features (see the next section), and (3) considering the energy injection required to create the shell at the distance given by the observed core radius from the Hα image. These three measurements point to the same conclusion, namely that the absolute number of massive stars, and therefore the assumed geometry, is consistent with observations in the three GEHRs studied.

5. DISCUSSION

5.1. *The Number of Wolf-Rayet Stars*

Once the metallicity, age, and mass of the cluster have been derived, it is possible to check that the model chosen for each region is adequate by deriving the number of W-R stars predicted by the model at this age and comparing the computed and observed luminosity of the W-R bumps at 4660 and 5810 Å.

We have used the isochrones from the Padova group to predict the absolute numbers of different types of W-R stars present in the theoretical H-R diagram of the cluster whose SED reproduces the nebular emission line spectrum. Using Figures 2*b* and 2*c* of GBD95a, we can predict the level of the optical emission in the W-R bumps. The predictions for the three GEHRs, A, B, and C, are shown in Table 4.

The next rows of Table 4 show the comparison between observed, L_o, and theoretical, L_t, luminosities for the bumps at 4660 and 5810 Å. The observed luminosities in the W-R

TABLE 4

ABSOLUTE NUMBERS OF MASSIVE STARS IN THE GEHRs

Region	A	B	C
WNL.....	25	40	59
WC.....	28	0	0
WNE.....	14	0	5
WO	0	0	7
$L_t(4660)$	38.2–38.3	37.9–38.1	38.1–38.3
$L_o(4660)$	38.2 ± 0.2–38.6 ± 0.2	38.0 ± 0.2–38.4 ± 0.2	37.8 ± 0.2–38.3 ± 0.2
$L_t(5810)$	38.0	36.7	36.9
$L_o(5810)$	38.1 ± 0.1–38.4 ± 0.1	<37.5	<37.5
$(\text{He II}/\text{H}\beta)_t$	0.02	0.01	0.01
$(\text{He II}/\text{H}\beta)_o$.....	0.02–0.05	0.01–0.04	0.0–0.03

NOTE.—The theoretical values of the He II/Hβ have been estimated according to the calculations by Schaerer 1996 for clusters between 3.5 and 4.5 Myr old and for the metallicities of the regions. The He II line luminosity has been taken as the 70% of the W-R luminosity band, considering a 30% contribution from N III lines.

bumps are the ones derived assuming that the reddening is either negligible or equal to the one derived for the gas from the recombination lines.

The theoretical luminosities have been calculated using the empirical calibrations by Smith (1991) and Vacca & Conti (1992). Smith (1991) gives average values for the luminosities in the W-R bumps. This calibration implies that a WNL produces $\log L_{4660}$ ergs $s^{-1} = 36.5$ and $\log L_{5810}$ ergs $s^{-1} = 35.1$, while a WC produces 36.7 and 36.5, respectively. We have considered Smith's calibration except for the WNL stars for which we have taken the most recent one used by Vacca & Conti (1992) based on an empirical calibration of the He II 4686 Å line for WNL in the LMC (Vacca 1991). They assume that the luminosity in this line for one WNL star is around 1.7×10^{36} ergs s^{-1}. The measured luminosity of the 4660 Å bump comprises the broad N III features at 4634, 4640, and 4642 Å, the narrow [Fe III] 4658 Å line, and the broad He II 4686 Å feature. The contribution to the total bump by the N III lines seems to be metallicity dependent (Smith 1991) and constitutes between 15% and 50% of the total. We have therefore added these contributions to the calculated He II luminosity value to provide lower and upper limits to the predicted total luminosity. Therefore, the expected value for the whole bump at 4660 Å (in logarithmic scale, with luminosity in ergs s^{-1}) ranges between 36.3 and 36.5. The two values listed in Table 4 for $L_t(4660)$ correspond to considering these two extreme values for the WNL stars.

For the studied regions, the discrepancies between the predicted and observed bumps (assuming the same reddening for the gas and for the stars) are less than a factor of 2. Several possibilities can be discussed. This difference could result from the signal-to-noise ratio in the optical spectra, which was not enough to measure the feature to better than a factor of 2 (the measured errors were 52%, 73%, and 49% for the W-R bump at 4660 Å for regions A, B, and C, respectively, and 31% for the bump at 5810 Å for region A). Alternatively, the average observed W-R features would be more consistent if no dust is associated with the cluster itself (the first value of the two given as L_o in Table 4). In this case, the possible explanation could be that the dust has been swept out from the central regions and has been mixed with the gas. This remains a matter for debate.

Recently, Schaerer (1996) has computed the ratio between the He II and Hβ emission lines for young stellar bursts as a function of the age and metallicity. His models include the nebular and stellar (He II from W-R) contribution to the lines. He uses the Geneva tracks and non-LTE blanketed atmosphere models, which take into account the stellar winds. We have compared his predictions for the studied regions assuming the metallicity and age we have derived. The Geneva and Padova evolutionary tracks lead to a slight difference in the age of the W-R stars, so the comparison is not straightforward, but nonetheless we have calculated the predicted value from his models for an age between 3.5 and 4.5 Myr to check if the models are roughly consistent. The predictions are also showed in Table 4.

We have calculated the observed ratio between the He II and Hβ. We have taken the He II luminosity considering that the N III broad lines contribute 30% to the total W-R luminosity band. Again, we give two extreme values; the lower one corresponds to considering no reddening associated with the star cluster, while the upper one corresponds to reddenning the stellar component with the same amount of dust derived for the gas. The agreement is very good and more consistent with the hypothesis of the *shell* scenario, in which the dust had been swept out from the stellar cluster.

5.2. *The Non-ionizing Population*

We have already shown that it is possible to explain the emission-line spectrum of the gas, the size of the region, and the W-R bumps on the basis of the existence of a very young, instantaneous starburst with an age between 3 and 5 Myr. In order to test whether this single population can be the only one present, three additional constraints were used: the equivalent width of the Hβ emission line, EW(Hβ); the continuum luminosity at 9000 Å, L_{9000}; and the presence or absence of the CaT in absorption.

The predicted EW(Hβ) values for the single star population ionizing each region are 110, 150, and 107 Å, respectively, for regions A, B, and C, larger than the observed ones by a factor of about 2 (Tables 5 and 6). There exists a well-known discrepancy between predicted and observed values of EW(Hβ) (see, e.g., Viallefond & Goss 1986) when nonevolving ionizing clusters are considered. In fact, only three of 425 H II galaxies in the catalog of Terlevich et al. (1991) show EW(Hβ) values comparable to the ones calculated for clusters younger than about 3 Myr (i.e., >350 Å; Mas-Hesse & Kunth 1991; GBD95b; Stasińska & Leitherer 1996). Under the assumption of single burst population and a radiation-bound nebula, an explanation for this disagreement can be found if the reddening affecting the emission

TABLE 5

OBSERVATIONS AND MODELS FOR REGIONS B AND C

PARAMETER	REGION B			REGION C		
	EW(Hβ) (Å)	L_{9000} (10^{37} ergs s^{-1} Å^{-1})	EW(CaT) (Å)	EW(Hβ) (Å)	(L_{9000} (10^{37} ergs s^{-1} Å^{-1})	EW(CaT) (Å)
Young	150	0.5–1.2	0.003	107	1.3–3.1	0.003
RSG-rich	...	0.5–1.2	0.003	...	1.7–4.1	0.003
Both	74	1.0–2.4	0.003	44	3.0–7.2	0.003
Observed	77	1.4	...	43	2.0	...
Corrected for internal extinction	171	2.1	...	112	3.2	...

NOTE.—EW(CaT) is the sum of the EW(Ca II) for the lines at 8542 and 8662 Å, in absorption. The contamination by the emission line Pa13 is only 0.5 Å (G95).

lines is caused by dust inside the regions (associated with the gas) and therefore does not affect the continuum of the ionizing clusters (Mayya & Prabhu 1996). If this is the case, the measured EW(Hβ) should be increased to 88, 171, and 112 Å for regions A, B, and C, respectively, close to the predicted values. In correcting the EW(Hβ) values, we have assumed that the nebular continuum amounts to 5% of the total cluster continuum for regions A and C and 8% for region B (see, e.g., García-Vargas, Mollá, & Bressan 1996) and that this nebular continuum is affected by the same reddening as the emission lines.

The ionizing populations produce a L_{9000} of 0.5×10^{37}, 0.5×10^{36} and 1.3×10^{37} ergs s^{-1} Å^{-1} for regions A, B, and C, respectively (see Tables 5 and 6). These numbers are calculated for a value of $m_{\rm low} = 0.85\ M_{\odot}$. Changing this value changes the calculated L_{9000} by the same amount as the total mass of the cluster (see § 3). The two entries given in the table correspond to values of $m_{\rm low}$ of 0.85 $M_{\odot}$ and 0.1 $M_{\odot}$. The nebular contribution to this continuum is 16%, 29%, and 35%. If we correct this nebular contribution for reddening [$E(B-V) = 0.24$, 0.27, and 0.33, respectively], these numbers change by 40%, since extinction is not very severe in the near-IR. However, for the calculations, we have considered that the nebular contribution to the spectrum is the one due to the number of photons derived from the Hα luminosity in the spectrum (not the total one we derived from the image).

The last row in Table 5 lists the observed L_{9000} values for every region. These numbers seem to imply a low value for lower mass cutoff of the IMF. However, it should be remembered that L_{9000} is a distance-dependent observable, and a 20% error in the distance determination would affect its value by 44% (we have used $H_0 = 75$ km s^{-1} Mpc^{-1}). Other factors, such as the error in the flux calibration of the near-IR spectrum, can affect the measured values.

Based on these arguments and on the observed values of the EW(Hβ) and the L_{9000}, we do not find any strong evidence for the contribution of a non-ionizing population for the observed regions. Two main assumptions are implied: (*a*) the nebula is ionization bound and (*b*) the observed extinction is internal to the H II region, and therefore affecting only the gas, and no dust is associated with the star cluster. A possible explanation could be that the dust has been swept out from the central regions and mixed with the gas.

If a different picture is assumed, i.e., if the observed extinction is supposed to be external to the region, then both star cluster and gas would be affected alike. Then, the discrepancy between predicted and observed EW(Hβ) would point either to an escape of ionizing photons from the nebula (matter-bound case), for which we do not find evidence as is discussed in § 4, or to the presence of a non-ionizing population in the GEHRs. Under this last assumption, in the following discussion, we will characterize this older component in the studied GEHRs.

The spectra of regions B and C show a rather featureless continuum and no absorption wings in the Balmer lines. Therefore, any non-ionizing population should be young enough not to contain red supergiants, since they would provide observable CaT strengths, and to contribute not more than 75% to the continuum at Hβ so that the absorption wings are not conspicuous. This constrains the age of this population between 5.5 and 9 Myr (these numbers depend only slightly on the metallicity). The existence of a two-burst population in each of these regions can be explained satisfactorily by the formation of a second burst when the first violent phenomena (strong winds from the most massive stars and supernovae) start to occur, around 4 Myr after the onset of the first burst. In fact, Mayya & Prabhu (1996), from a study of 35 GEHRs, find that 75% of

TABLE 6

OBSERVATIONS AND MODELS FOR REGION A

Parameter	EW(Hβ) (Å)	L_{9000} (10^{37} ergs s^{-1} Å^{-1})	EW(CaT) (Å)
Young (5 Myr)	110	0.5–1.2	0.01
RSG-rich (9 Myr)	...	4.1–9.8	6.1
(1) 5 My+9 Myr	45	4.6–11.0	4.4
(2) Bulge + 5 Myr	49	12.4–13.1	6.6
(3) Bulge + 5 Myr + 9 Myr	11	29.4–35.8	5.5
Observed	45	3.7	4.5
Corrected for internal extinction	88	5.2	4.5

NOTE.—The bulge in the composite models has been considered to be a 10 Gyr population at half-solar metallicity.

the sample contains stars from more than one burst over the last 10 Myr and that the most recent burst has occurred within the last 3 Myr in 90% of these regions.

Therefore, to model each of these two regions, B and C, we have considered two successive bursts of the same mass, the second one occurring 4 Myr after the first one. Populations of 3.5 and 7.5 Myr in region B and 4.5 and 8.5 Myr in region C have been combined to reproduce the observations. These older populations, contributing 50% and 40%, respectively, to the continuum at Hβ would lower the predicted values of EW(Hβ) to 74 and 44 Å, respectively, while increasing L_{9000} to $(1.0\text{–}2.4) \times 10^{37}$ and $(3.0\text{–}7.2) \times 10^{37}$ ergs s^{-1}; the two values are for the different $m_{\rm low}$ assumed, still consistent with observations (see Table 5) and a value of $m_{\rm low}$ of about 0.85 $M_{\odot}$.

Turning now to region A, note that this region, as already mentioned, is located close to the galactic nucleus and could be in the bulge because it is located in the rising, solid body rotation part of the velocity curve (see Figs. 6*a* and 15*a* in G95). Therefore, some contamination from an underlying population cannot be excluded.

In fact, the spectrum of region A (see Fig. 5*b* in G95) exhibits absorption lines of Ca II (3933 Å), Mg I (5172, 5183 Å), Fe I (4383, 5269, 5330 Å), Na I (5896 Å), Na I (8192 Å), and Ca II, CaT (8498, 8542, 8662 Å), and a TiO band around 6300 Å. CaT and TiO features are compatible with both an old metal-rich bulge population (10 Gyr) and a young population, rich in red supergiants (Bica & Alloin 1987; see also as an example the cluster NGC 2002 in the LMC, with an age between 7 and 12 Myr, showing both features; Fig. 7 in Bica, Alloin, & Santos 1990a).

Moreover, from the spatial distribution of the continuum in a narrow-band image near Hα (at 6925 Å; see Fig. 1*d* in G95), it can be inferred that the local continuum under region A represents only 30% of the total. If the underlying population contributing the remaining 70% were an old metal-rich population, it would provide about 6 Å equivalent width of the Mg I line (see, e.g., Bica & Alloin 1986b) while the measured value is only 1.5 Å. Even an old metal-poor population, like that corresponding to a galactic globular cluster, would produce an EW(Mg I) of 5 Å (Bica & Alloin 1986a, 1986b). Moreover, such an old underlying population would produce a L_{9000} a factor of 5 much larger than observed. Furthermore, wide absorption wings in the Balmer lines are observed in the spectrum of region A, which would not be accounted for by an old population.

The underlying population can still correspond to a relatively young one. Young LMC clusters (between 8 and 25 Myr) and metallicity 0.5 solar have EW(Mg I) of the order of 2 Å (see Bica & Alloin 1986a, 1986b). Based on the colors published by Bica & Alloin, such a population would provide the observed Mg I strengths and around 85% of the total luminosity at 9000 Å. Clusters as old as 20 Myr would provide too much continuum at Hβ, producing small equivalent widths (of the order of 14 Å), but a cluster with 9 Myr would fit the observations, as can be seen from Table 6. Such a population can also explain the wings observed in the Balmer lines (Díaz 1988).

To support our explanation of the coexistence of two bursts of star formation, we have to investigate the behavior of the only one feature from red supergiant stars (RSGs) strong enough to be measured in the spectra, the CaT in the near-IR. There are very few GEHRs in which this feature has been detected. In fact, it is not always clear whether the CaT is produced by RSGs or by the giants present in the old, bulge population (see the discussion in Terlevich et al. 1996; García-Vargas et al. 1997 and references therein). Thus, modeling the stellar population, whose combination can reproduce all the observables, becomes a key issue.

The CaT in the near-IR ($\lambda\lambda$ 8498, 8542, 8662 Å) is produced by giant or supergiant red stars. For red giants and supergiants, the equivalent width of these absorption lines depends on the metallicity and on the gravity of the stars. At high metallicity ($Z > 0.5\ Z_{\odot}$), the depth of the lines depends mainly on the gravity, and EW(CaT) values larger than 7 Å are found only in red supergiant stars (Díaz, Terlevich, & Terlevich 1989; Zhou 1991). However, for cool red giants, the effective temperature can play an important role, too, and the CaT behavior becomes triparametric in ($T_{\rm eff}$, log g, Z) (Zhou 1991; Jørgensen, Carlsson, & Johnson 1992; Mallik 1994).

Recently, García-Vargas et al. (1997) have computed theoretical models in which the EW(CaT) is calculated for single and combined populations, over a wide range of ages (from very young clusters to bulge populations). The theoretical calibrations by Jørgensen et al. (1992) and data from Díaz et al. (1989) and Zhou (1991) were used to calculate the synthetic equivalent widths of CaT for the H-R diagrams of single stellar populations computed with Padova's isochrones for ages between 1 and 15 Gyr. From these models, the highest values for CaT in bulge, solar metallicity populations are around 6.5 and 7 Å. For lower metallicities, both, stellar populations and the index itself, point to lower values of CaT.

Here, we explore three different models for region A: (1) a two-burst model, just as in regions B and C, with the same contribution in mass and considering ages of 5 and 9 Myr, the older burst being rich in RSG; (2) a model in which the ionizing population plus an underlying bulge of 10 Gyr are considered; and (3) a model in which the two bursts (5 and 9 Myr) plus the bulge (10 Gyr) are taken into account.

The underlying population contribution has been inferred from the spatial distribution of the continuum in a narrow-band image near Hα as has been explained above. If this underlying population was an old bulge, and from the synthetic SED corresponding to a 10 Gyr population, we have calculated its contributions at the Hβ and CaT continuum, and at 9000 Å, and we have weighted the populations accordingly. For the underlying population taken into account in these models, the contribution in mass is around 99%. This result agrees with the simulations by Bica, Alloin, & Schmidt (1990b), where they combine old populations with young bursts to reproduce different types of nuclear region spectra. For the case most similar to region A, these authors obtain a mass contribution from the star-forming burst of around 1%. In fact, similar to their results, we find that if an old bulge population contributes in mass less than 91%, its effect on the integrated light properties becomes negligible, and the dominant light contribution would be from the rich-RSG component.

Table 6 shows the results of the models for region A. The model that best reproduces the observations is the two-burst model (model 1), which fits simultaneously EW(Hβ), EW(CaT), and L_{9000}. If an old (10 Gyr) bulge is considered (model 2), the predicted values for EW(CaT) and EW(Hβ) are consistent with the observations although not as consistent as in model 1 but still within the error bars, but it is not consistent with the observed L_{9000} or with other spectral

features, such as the observed strength of the Mg I line or the wings observed in the Balmer lines as discussed above. If both a RSG-rich and a bulge population are taken into account (model 3), the predicted value for EW(Hβ) would be definitively too low. Moreover, both models including an old bulge (models 2 and 3) predict values of L_{9000} that are excessively large. For these calculations, the metallicity of the bulge has been taken to be half-solar. If a metal-rich bulge (around solar) was considered, then the computed EW(CaT) would be even higher (around 6–6.5 Å) for models including the bulge contribution, and the comparison with observations would be even less satisfactory.

According to our results, the model for region A is consistent with the existence of two populations, the ionizing one with an age of 5 Myr, and an older one, of 9 Myr, RSG-rich, and therefore responsible for the dilution of the Hβ equivalent width, the presence of CaT, the rest of the spectral features, and also for the component in absorption seen in the Balmer lines. A high-resolution spectroscopic study (including the measurement of the velocity dispersion from CaT in the nucleus and in region A) will be needed to determine if this older component belongs to the region or to the extended nuclear starburst.

6. SUMMARY AND CONCLUSIONS

The aim of this paper was to demonstrate how we can analyze the stellar content of a GEHR through the observation of its ionized gas. In fact, we have shown that it is possible to explain the optical emission-line spectrum of the gas, the W-R bumps, and the size of three circumnuclear GEHRs in the starburst galaxy NGC 7714 by considering a very young, ionizing burst of star formation, with age between 3 and 5 Myr. We have used an evolutionary synthesis code to model the burst. The SED of the young stellar population is the input into the photoionization code CLOUDY, which is used to fit the nebular spectrum and hence to constrain the main physical properties, such as mass, age, and metallicity of this young population.

However, for regions B and C, and when other observations, not directly related to the most massive stars in the burst, such as the EW(Hβ) and L_{9000} in the near-IR, are taken into account, some hypothesis about the dust distribution (internal to the region and therefore not affecting the cluster continuum) or the presence of a previous burst, between 8.5 and 12 Myr, become necessary. The mechanism we propose to explain the first possibility is that the winds from massive stars have swept out the dust from the cluster and it has been mixed with the gas. With respect to the second solution, if an older population is assumed, the triggering of this second burst of star formation occurring when supernovae from massive stars in the initial burst begin to explode is a natural mechanism we envisage to explain the existence of at least two bursts in regions B and C.

In the case of region A, we have also proposed the existence of an older underlying component, for which we have found direct evidences in the spectrum, such as Mg I and other features in the blue, TiO bands in the red, and Na I and CaT in the near-IR. The nature of this population has also been discussed. An old (10 Gyr) metal-rich bulge cannot explain the observations, and the inclusion of a rich RSG population is necessary. Whether this population belongs to the region itself, and therefore coexists with the ionizing one, or not, can be determined from future observations, in particular by determining the velocity dispersion from the CaT lines. Finally, we outline the importance of similarly detailed studies in other GEHRs, because they are the simplest and most useful laboratories of star formation in which the models can be tested, with many observational constraints being available.

We thank Gary Ferland for kindly making his code available. We are grateful to the Comité Científico Internacional for allocating 5% of the observing time at the Observatorio del Roque de los Muchachos to the GEFE collaboration. The 4.2 m William Herschel and 1 m Jacobus Kapteyn telescopes, on which the data used for this work were obtained, are operated by the Royal Greenwich Observatory at the Spanish Observatorio del Roque de los Muchachos of the Instituto de Astrofísica de Canarias. M. García-Vargas, E. Pérez, & R. González-Delgado are grateful to the Instituto de Astrofísica de Canarias and to the Space Telescope Science Institute for the kind support provided during part of the realization of this work. We have benefited from helpful discussions with Claus Leitherer, Miguel Mas-Hesse, Casiana Muñoz-Tuñón, J. A. Rodríguez-Gaspar, Daniel Schaerer, and Guillermo Tenorio-Tagle. We also thank the anonymous referee for the useful comments which have contributed significantly to the improvement of the paper. This work has been partly financed by DGICyT grants PB91-0531 (GEFE) and PB93-0139 and by INSA.

REFERENCES

Avedisova, V. S. 1972, Soviet Astron.—AJ, 15, 708
Bica, E., & Alloin, D. 1986a, A&A, 162, 21
———. 1986b, A&AS, 66, 171
———. 1987, A&A, 186, 49
Bica, E., Alloin, D., & Santos, J. F. C., Jr. 1990a, A&A, 235, 103
Bica, E., Alloin, D., & Schmidt, A. 1990b, MNRAS, 242, 241
Bernlöhr, K. 1993, A&A, 268, 25
Bressan, A., Bertelli, C., & Chiosi, C. 1981, A&A, 102, 25
Bressan, A., Fagotto, F., Bertelli, G., & Chiosi, C. 1993, A&AS, 100, 647
Castor, J., McCray, R., & Weaver, R. 1975, ApJ, 200, L107
Clegg, R. E. .S., & Middlemass, D. 1987, MNRAS, 228, 759
Courtes, G., Petit, H., Sivan, S. P., Dododnov, S., & Petit, M. 1987, A&A, 174, 28
Cox, D. P. 1972, ApJ, 178, 159
de Jager, C., Nieuwenhuijzen, H., & van der Hucht, K. A. 1988, A&AS, 72, 259
Demoulin, M. 1968, ApJ, 153, 31
Díaz, A. I. 1988, MNRAS, 231, 57
———. 1994, in Star Formation from 30 Dor to QSOs, ed G. Tenorio-Tagle (Cambridge: Cambridge Univ. Press), 105
Díaz, A. I., Terlevich, E., & Terlevich, R. 1989, MNRAS, 239, 325
Díaz, A. I., Terlevich, E., Vílchez, J. M., Pagel, B. E. J., & Edmunds, M. G. 1991, MNRAS, 253, 245
Dyson, J. E. 1979, A&A, 73, 132
Fagotto, F., Bressan, A., Bertelli, G., & Chiosi, C. 1994a, A&AS, 104, 365
———. 1994b, A&AS, 105, 29
Falle, S. A. E. G. 1975, A&A, 43, 323
Ferland, G. J. 1991, HAZY, a Brief Introduction to CLOUDY, v. 80.08
García-Vargas, M. L. 1996, in ASP Conf. Proc. 98, From Stars to Galaxies: The Impact of Stellar Physics on Galaxy Evolution, ed. C. Leitherer, U. Fritze–von Alvensleben, & J. Huchra (San Francisco: ASP), 244
García-Vargas, M. L., Bressan, A., & Díaz, A. I. 1994, in Star Formation from 30 Dor to QSOs, ed G. Tenorio-Tagle (Cambridge: Cambridge Univ. Press), 133
———. 1995a, A&AS, 112, 13 (GBD95a)
———. 1995b, A&AS, 112, 35 (GBD95b)
García-Vargas, M. L., & Díaz, A. I. 1994, ApJS, 91, 553
García-Vargas, M. L., Mollá, M., & Bressan, A. 1997, A&AS, submitted
Garnett, D. R. 1989, ApJ, 345, 282

González-Delgado, R. M., & Pérez, E. 1996, MNRAS, in press
González-Delgado, R. M., Pérez, E., Díaz, A. I., García-Vargas, M. L., Terlevich, E., & Vílchez, J. M. 1995, ApJ, 439, 604 (G95)
Hunter, D. A. 1994, AJ, 106, 1658
Hunter, D. A., Boyd, D. M., & Hawley, W. M. 1995, ApJS, 99, 551
Iglesias, C. A., Rogers, F. J., & Wilson, B. G. 1992, ApJ, 397, 717
Jørgensen, U. G., Carlsson, M., & Johnson, H. R. 1992, A&A, 254, 258
Kudritzki, R. P., Pauldrach, A., & Puls, J. 1987, A&A, 173, 293
Kurucz, R. 1992, in IAU Symp. 149, The Stellar Populations of Galaxies, ed. B. Barbury & A. Renzini (Dordrecht: Kluwer), 225
Langer, N. 1989, A&A, 210, 93
Leitherer, C., & Heckman, T. M. 1995, ApJS, 96, 9
Leitherer, C., Robert, C., & Drissen, L. 1992, ApJ, 401, 596
Leitherer, C., Vacca, D., Conti, P., Filippenko, A. V., Robert, C., & Sargent, W. L. W. 1996, ApJ 465, 717.
Maeder, A. 1991, A&A, 242, 93
Mallik, S. V. 1994, A&AS, 103, 279
Mas-Hesse, J. M., & Kunth, D. 1991, A&AS, 88, 399
Mayya, Y. D., & Prabhu, T. P. 1996, AJ, 111, 1252
McCall, M. C., Rybski, P. M., & Shields, G. A. 1985, ApJS, 57, 1
McGaugh, S. S. 1991, ApJ, 380, 140
Osterbrock, D.E. 1989, Astrophysics of Gaseous Nebulae and Active Galactic Nuclei (Mill Valley: University Science Books)
Osterbrock, D. E., Tran, H. D., & Veilleux, S. 1992, ApJ, 389, 196
Pelat, D., Fosbury, R. A. E., & Alloin, D. 1981, MNRAS, 195, 787
Perez, E., et al. 1997, in preparation
Rosado, M., Laval, A., LeCoarer, E., Georgelin, Y. P., Amram, P., Marcelin, M., Goldes, G., & Gach, J. L. 1996, A&A, 308, 588
Salpeter, E. E. 1955, ApJ, 121, 161
Schaerer, D. 1996, ApJ, 467, L17
Smith, L. F. 1991, in IAU Symp. 143, Wolf-Rayet Stars and Interrelations with Other Massive Stars in Galaxies, ed. K. A. van der Hucht & B. Hidayat (Dordrect: Kluwer), 601
Stasińska, G. 1990, A&AS, 83, 501
Stasińska, G., & Leitherer, C. 1996, ApJS, 107, 661
Stevenson, C. C. 1994, MNRAS, 267, 904
Terlevich, E., Díaz, A. I., Terlevich, R., González-Delgado, R. M., Pérez, E., & García-Vargas, M. L. 1996, MNRAS, 279, 1219
Terlevich, R., Melnick, J., Masegosa, J., Moles, M., & Copetti , M. V. F. 1991, A&AS, 91, 285
Vacca, W. D. 1991, Ph.D. thesis, Univ. Colorado, Boulder
Vacca, W. D., & Conti, P. S. 1992, ApJ, 401, 543
Viallefond, F., & Goss, W. M. 1986, A&A, 154, 357
Weaver, R., McCray, R., Castor, J., Shapiro, P., & Moore, R. 1977, ApJ, 218, 377
Weedman, D. W., Felman, F. R., Balzano, V. A., Ramsey, L. W., Sramek, R. A., & Wu, C. C. 1981, ApJ, 248, 105
Zhou, X. 1991, A&A, 248, 367